SCIENTIFIC REPORTS

OPEN

SUBJECT AREAS:
NANOPHOTONICS AND PLASMONICS
SUB-WAVELENGTH OPTICS

Received
28 October 2014

Accepted
29 December 2014

Published
23 January 2015

Correspondence and requests for materials should be addressed to D.D. (dxdai@zju.edu.cn)

Tunable pattern-free graphene nanoplasmonic waveguides on trenched silicon substrate

Jiajiu Zheng, Longhai Yu, Sailing He & Daoxin Dai

Centre for Optical and Electromagnetic Research, State Key Laboratory for Modern Optical Instrumentation, Zhejiang Provincial Key Laboratory for Sensing Technologies, Zhejiang University, Zijingang Campus, Hangzhou 310058, China.

Graphene has emerged as a promising material for active plasmonic devices in the mid-infrared (MIR) region owing to its fast tunability, strong mode confinement, and long-lived collective excitation. In order to realize on-chip graphene plasmonics, several types of graphene plasmonic waveguides (GPWGs) have been investigated and most of them are with graphene ribbons suffering from the pattern-caused edge effect. Here we propose a novel nanoplasmonic waveguide with a pattern-free graphene monolayer on the top of a nano-trench. It shows that our GPWG with nanoscale light confinement, relatively low loss and slowed group velocity enables a significant modulation on the phase shift as well as the propagation loss over a broad band by simply applying a single low bias voltage, which is very attractive for realizing ultra-small optical modulators and optical switches for the future ultra-dense photonic integrated circuits. The strong light-matter interaction as well as tunable slow light is also of great interest for many applications such as optical nonlinearities.

Plasmonics has been regarded as one of the most promising strategies to realize light manipulation on nanoscale[1]. Noble metals, like silver and gold, are used popularly as the dominant materials for plasmonics because of their capability of supporting the surface plasmon polaritons (SPPs) at visible and near-infrared wavelengths. However, there is a great challenge for noble metals' application in actively tuning plasmonic devices[2] due to the difficulty in modifying their permittivity. Current active plasmonic devices are usually realized with the assistance of another active optical material[3–5].

Recently, graphene, a two-dimensional (2D) material of carbon atoms arranged in a honeycomb lattice, has been recognized as an excellent candidate for realizing inexpensive, fast, and compact active plasmonic devices with reduced power consumption at ambient conditions[6]. This is attributed to the intriguing properties of graphene surface plasmons (GSPs)[6–10]. First, the Fermi level E_F relative to the Dirac point and correspondingly the optical properties of graphene can be tuned synchronously and locally via chemical doping or electrical gating due to its two-dimensional nature[11–13]; Second, GSPs show strong mode confinement and slow group velocity with its GSP wavelength two orders smaller than that in free space[14–17]; Third, GSPs potentially provide smaller losses and therefore longer propagation lengths in comparison with surface plasmons in noble metals[18] because of graphene's long relaxation time related to high carrier mobility μ (Ref. 19); Furthermore, GSPs mainly lie in the THz to MIR region[10] where there are various significant applications for spectroscopy, chemical and biological sensing, imaging, and communications, etc[20].

In order to realize on-chip graphene plasmonics, the fundamental is to make an excellent waveguide. People have proposed several types of graphene plasmonic waveguides (GPWGs)[9,18,21–28] and most of them are made with graphene ribbons[18,21,22,25,26]. However, the edge scattering effect and band gap opening in a graphene ribbon introduce extra plasmon damping to GSPs[18,29]. Therefore, a GPWG with a pattern-free graphene monolayer is preferred. This can be realized via creating customized conductivity patterns by employing the tunability of graphene. For example, separated gating pads can be introduced so that different bias voltages can be applied to the graphene monolayer in different positions[9,27]. However, the electrical operation for the gating pads is complicated due to more than one pads involved, particularly when two or more waveguides are placed close to each other (which is necessary for lots of photonic integrated devices). A patterned spacer layer can also be utilized by introducing a nano-ridge structure[9,23,24] or more than one materials[9] such that only one gate voltage is needed. One should note that the fabrication for the spacer with different materials is not convenient. For the design with a nano-ridge[9,23,24], the transverse magnetic (TM) SPP mode is only supported in the core region. In other words,

there is no TM SPP mode supported in the side-cladding region. In this case, the aspect ratio of the nano-ridge is as high as ~10 according to Ref. 9, which makes the fabrication hard.

Here we propose a novel nanoplasmonic waveguide with pattern-free graphene by introducing a spacer with a reversed nano-ridge (which is formed by etching a nano-trench on the doped silicon substrate). Unlike GPWGs reported in Ref. 9, 23, 24, the graphene surface of the proposed structure in both the core and the side-cladding regions supports the TM SPP modes with very distinct effective indices so that tight lateral confinement can be achieved. When the gate voltage varies, the Fermi levels of the graphene monolayer in the core and the side-cladding regions are modified accordingly. In this way, a significant modulation on the phase shift as well as the propagation loss over a broad band is achieved by simply applying a single low bias voltage, which is very favorable to realize some key dynamic elements including ultra-small optical modulators and optical switches, as presented in this paper. In addition, the fabrication for the proposed structure is relatively easy since the aspect ratio of the nano-trench is only 0.2 ~ 1.5.

Structure and Results

As shown in Figure 1(a), the proposed tunable GPWG has a doped silicon substrate with a nano-trench, an Al_2O_3 spacer, a pattern-free graphene monolayer on the top, and an Al_2O_3 upper-cladding for protection. In this structure, GSPs are guided in the surface of the pattern-free graphene monolayer. The Al_2O_3 spacer has a flat top-surface and consequently the spacer has different thicknesses (d_1 and d_2) in the trenched and non-trenched regions, i.e., $d_1 > d_2$. Therefore, when a gate voltage V_G is applied, the graphene in the trenched region has a lower Fermi level and higher SPP effective index n_{eff} than that in the non-trenched region according to the relationships of $E_F \propto (V_G/d)^{1/2}$ and $n_{eff} \propto (d/V_G)^{1/2}$ (see Methods). In this way, graphene is electrostatically patterned to form a GPWG enabling strong light confinement on nanoscale, as confirmed by the calculated typical electric field profile of the fundamental SPP mode in the proposed GPWG [see Fig. 1(b)]. The operation frequency considered in the following investigations is $f = 37.5$ THz. In this example, the parameters are $w = 100$ nm, $d_1 = 60$ nm, $d_2 = 40$ nm, and $V_G = 7.2$ V. Correspondingly, one has $E_{F1} = 0.3$ eV and $E_{F2} = 0.37$ eV (see Methods). Here we assume that the graphene monolayer for the proposed trenched graphene nanoplasmonic waveguide has a *stepped* Fermi level distribution at the boundary between the trenched and non-trenched regions in a similar way shown in Ref. 9, 27. Accurate prediction for the carrier concentration and the Fermi-level distributions in graphene can be achieved with the electrostatic field distribution calculated numerically[23,24].

In order to better understand the SPP mode supported in the proposed GPWG, we show the calculated effective indices Real(n_{eff}) for the fundamental mode as well as the higher-order modes as a function of the waveguide width w in Fig. 2(a). It can be seen that the guided-modes have very large effective indices varying from ~37 to ~67 and there are five modes supported even when the width is as small as $w = 300$ nm. In order to be single mode, the core width w should be smaller than 50 nm, which definitely helps to achieve ultra-high integration density. The propagation loss (dB/μm) for the guided-modes in the proposed GPWG is given in Fig. 2(b). It shows that the propagation loss is 2 ~ 6 dB/μm originating from the light interaction with the lossy graphene in the core region as well as in the side-cladding region. Consequently, it is not a good option for long-distance propagation, which is a common issue for almost all surface nanoplasmonic waveguides. Fortunately, the functionality elements based on the proposed GPWG could be very short because the ultra-high effective index [see Fig. 2(a)] makes it possible to achieve π phase-shift within ~100 nm. Consequently, the excess loss of such ultra-short functionality elements is still acceptable, e.g. ~1 dB or less. We also note that there is a maximum for the propagation loss of any guided-mode as the core width increases. In order to explain this, one should note that the present GPWG has three regions with different material losses (i.e., the graphene in the core region, the graphene in the side-cladding region, and the lossless upper-/under-claddings) and the GP in the side-cladding region has lower propagation loss due to the higher Fermi level in comparison with the GP in the core region according to Eq. (2) (see Methods). Taking the fundamental mode as an example, the propagation loss becomes maximal around $w = 90$ nm. When the core width is large ($w > 200$ nm), the present GPWG behaves like a slab waveguide (i.e., $w \to \infty$). In this case, light is mainly confined in the core region and interacts with the graphene in this region strongly, so that the propagation loss is not sensitive to the core width and approaches the loss for the slab waveguide. As the core width decreases from 200 nm to 90 nm, our calculation shows that the power confinement factor (the fraction of power flowing in the region of interest[30]) of the graphene in the core region and the side-cladding increases slightly, which indicates a stronger light-graphene interaction and thus

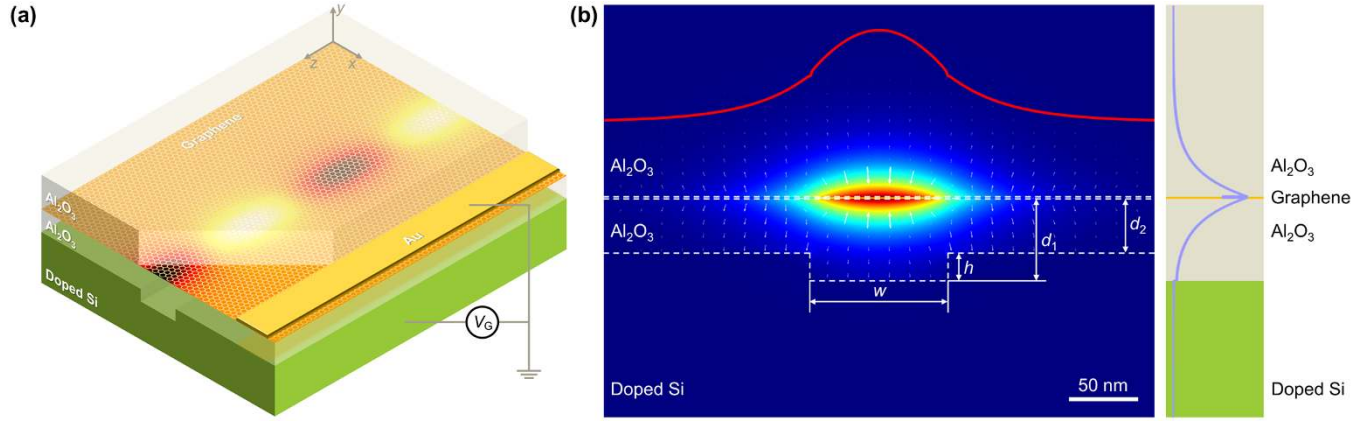

Figure 1 | The present novel tunable MIR GPWG. (a) Three-dimensional schematic of the proposed waveguide along with the E_z component of the propagating GSP mode. The gate voltage V_G is applied between the doped silicon and the gold electrode placed on top of graphene. (b) Left: x-y plane cross-section of the waveguide in (a) with an overlay of the total electric field profile of the fundamental mode when $w = 100$ nm, $d_1 = 60$ nm, $d_2 = 40$ nm, and $V_G = 7.2$ V (correspondingly the Fermi levels for the graphene in the core and cladding regions are $E_{F1} = 0.3$ eV and $E_{F2} = 0.37$ eV, respectively). The white dashed lines indicate the boundary of different materials and the white arrows shows the x-y plane electric field vector. The red curve illustrates the magnitude of the electric field across the graphene monolayer. Right: cross-section through the centre of the waveguide with the purple curve showing the magnitude of the electric field.

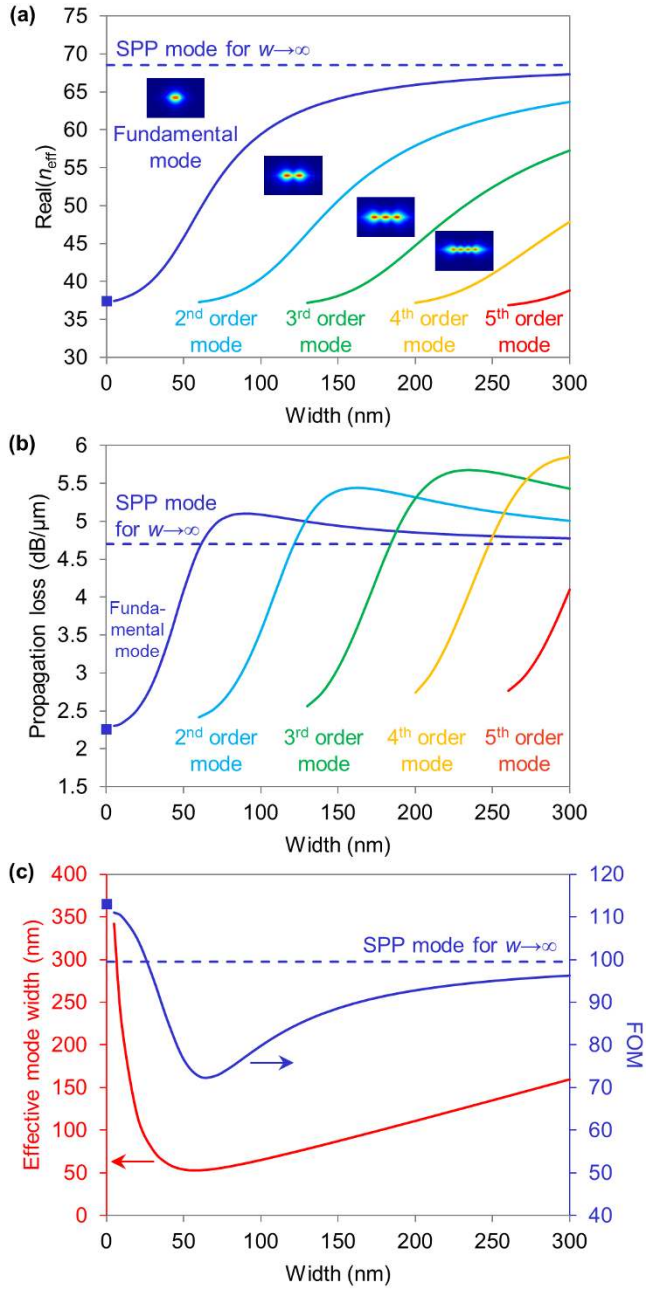

Figure 2 | Width dependence of (a) the real part of the effective index, Real(n_{eff}), (b) the propagation loss, and (c) the effective mode width and FOM for the proposed GPWG when $d_1 = 300$ nm, $d_2 = 100$ nm, $E_{F1} = 0.3$ eV, and $E_{F2} = 0.52$ eV. The insets of (a) display typical electric field profiles for the guided-modes. The squares and dashed lines indicate the values when $w = 0$, and $w \to \infty$, respectively.

results in a slight increase of the propagation loss. When the core width decreases further ($w < 90$ nm), more field extends into the side-cladding region, and thus the contribution to the whole propagation loss from the light interaction with the graphene at the side-cladding becomes more and more dominant, which results in a reduction of the propagation loss. As a consequence, it is expected to have a maximum for the propagation loss of the fundamental mode, as shown in Fig. 2(b). Figure 2(c) shows the calculated effective mode width for the fundamental mode of the present GPWG. It is notable that the minimal effective mode width is as small as 53 nm to enable nanoscale light confinement and guiding. In order to synthetically evaluate the loss and the confinement ability of the present waveguide, the figure of merit (FOM) defined as Re(β)/Im(β) is also calculated and shown in Fig. 2(c). It is found that FOM ranges from 70 to 110 as the core width varies and there is a valley around $w =$ 60 nm. One should choose the waveguide width appropriately by making a trade-off between the propagation loss and the effective mode width.

For the present GPWG, the spacer thickness d_2 also plays an important role, as shown in Fig. 3(a). As d_2 varies, the ratio d_1/d_2 is fixed as 3 here and the Fermi levels can be kept unchanged by tuning the applied gate voltage appropriately according to the relationship $E_F \propto (V_G/d)^{1/2}$ so that the equivalent dielectric constant of graphene does not change. For the present example, we choose $w = 100$ nm, $E_{F1} = 0.3$ eV, and $E_{F2} = 0.52$ eV. When the spacer is very thin ($d_2 < 5$ nm), the silicon substrate which has a larger dielectric constant than the Al_2O_3 spacer can "see" the modal field more and consequently, Real(n_{eff}) becomes sensitive to the spacer thickness d_2. This is why Real(n_{eff}) of the fundamental mode decreases very quickly from ~480 to ~65 when d_2 increases from zero to 5 nm, as show in Fig. 3(a). When $d_2 >$ 5 nm, Real(n_{eff}) becomes insensitive to the variation of d_2 because little field penetrates into the silicon substrate. We also note that when d_2 increases from zero, the propagation loss quickly decreases from ~18 dB/μm to the minimum ~4 dB/μm (located at $d_2 =$ ~5 nm) and then increases slightly to 5 dB/μm. One should note that the spatial dispersion (tensor conductivity) and the quantum capacitance should be taken into account[31,32] for achieving accurate estimation of the value Real(n_{eff}) and the propagation loss when d_2 is ultrathin (e.g., ~3 nm).

In order to further understand the dependence of Real(n_{eff}) and the propagation loss on d_2, we make an equivalent slab waveguide [see Fig. 3(b)] for the present GPWG by using the effective index method (EIM, see Methods), which has been used very often to make the calculation efficient and to help understand the mode properties. Figure 3(c) shows the real part and imaginary part of the calculated indices (n_{eff_co}, n_{eff_cl}) for the core and the cladding layers of the equivalent three-layer slab waveguide for the present GPWG, both of which decrease quickly and eventually approach the values for $d_2 \to \infty$ as d_2 increases. This is expected from Eq. (2) (see Methods) when the silicon substrate (which has a larger dielectric constant than the Al_2O_3 spacer) is separated farther. The index contrast defined as Real(n_{eff_co}) – Real(n_{eff_cl}) is also shown in the inset of Fig. 3(a), which reaches the minimum when $d_2 \approx 3$ nm and the effective mode width of the GPWG is expected to have a maximum correspondingly. As the mode field profile is significantly dependent on the index contrast, the power confinement factor in the core layer also becomes minimal around $d_2 \approx 3$ nm. Because the core layer of the equivalent three-layer slab waveguide dominates the total propagation loss [see the imaginary parts of n_{eff_co} and n_{eff_cl} shown in Fig. 3(b)], the equivalent three-layer slab waveguide also has a minimal propagation loss around $d_2 \approx 3$ nm, as shown by the dashed line in Fig. 3(a). The results for the equivalent three-layer slab waveguide (from EIM) agree very well with those for the GPWG (from FEM), which indicates that EIM can give reasonably accurate calculation for the present GPWG. This is very helpful for simplifying the simulation of the present GPWG, particularly for the simulation of light propagation along the GPWG circuits.

According to Fig. 3(a), we choose $d_2 = 40$ nm for the design given below in order to have a large tolerance for the thickness d_2. Figure 4(a) shows how the Fermi levels (E_{F2}, and E_{F1}) influences the fundamental mode of the GPWG with $w = 100$ nm and $d_2 =$ 40 nm. For this calculation, E_{F1} for the core is fixed to be 0.2 eV, 0.3 eV, and 0.4 eV by adjusting the applied gate voltage accordingly while E_{F2} for the cladding is modified by choosing the thickness d_1 appropriately to make the ratio E_{F2}/E_{F1} vary in the range from 1.0 to 2.0. It can be seen that one has a smaller the effective mode width when choosing lower E_{F1}. Figure 4(a) also shows that the effective mode width decreases steeply when E_{F2}/E_{F1} increases from 1.0. The

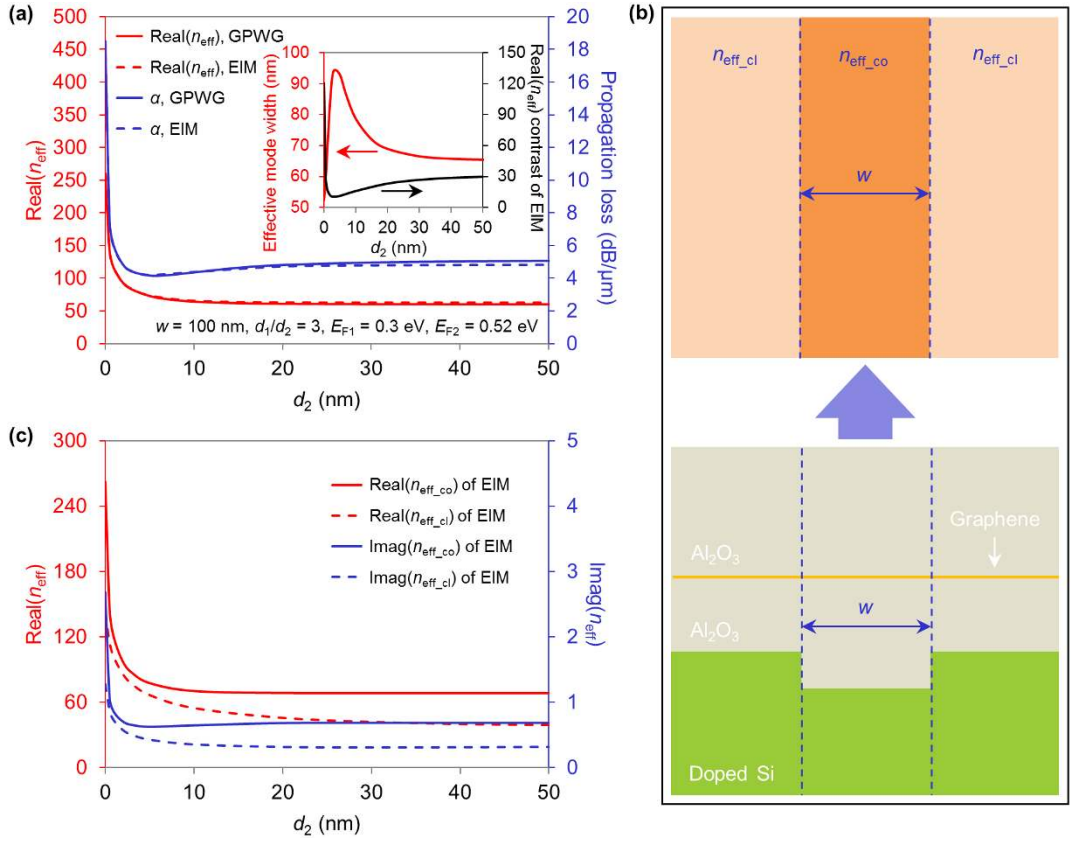

Figure 3 | Mode properties of the proposed GPWG as the spacer thickness d_2 varies. (a) Real(n_{eff}), and the propagation loss, the effective mode width (inset), and the index contrast of the equivalent slab waveguide with the assistance of EIM (inset) as a function of d_2 when w = 100 nm, d_1/d_2=3, E_{F1} = 0.3 eV, and E_{F2} = 0.52 eV. (b) The equivalent three-layer slab waveguide from EIM (see Methods for details). (c) The real part and imaginary parts of the indices for the core (solid lines) and the cladding (dashed lines) of the three-layer equivalent slab waveguide.

reason is that the index contrast is larger when choosing lower E_{F1} or higher E_{F2} according to Eq. (2) (see Methods). More importantly, when E_{F2}/E_{F1} increases from 1.0, the index contrast increases quickly to be so large that the effective mode width is determined mainly by the core width. As a result, the effective mode width becomes insensitive to this ratio when E_{F2}/E_{F1} becomes slightly larger than 1.0 (e.g. $E_{F2}/E_{F1} > 1.2$). For example, for the case of E_{F1} = 0.3 eV, the effective mode width decreases from 345 nm to 105 nm when E_{F2}/E_{F1} increases from 1.0 to 1.1. When the ratio increases further, the effective mode width decreases very slightly. This indicates that a deep trench is not necessary to a GPWG with strong lateral confinement and consequently, the fabrication is easy.

Figure 4(b) illustrates Real(n_{eff}) and the propagation loss of the fundamental mode as the Fermi level E_{F1} for the graphene in the core region varies by modifying the gate voltage. For this calculation, we choose w = 100 nm, d_1 = 60 nm, d_2 = 40 nm to make $E_{F2}/E_{F1} = 1.5^{1/2}$ as an example. It shows that Real(n_{eff}) (or phase shift) as well as the propagation loss can be modulated significantly by introducing a small variation of the gate voltage. As a result, it is potential to build an optical modulator of phase or amplitude with an ultra-small footprint, which is helpful to achieve ultra-high speed. In this paper, we consider the design for an optical modulator of amplitude given the structural simplicity. As the insertion loss and the extinction ratio are the two key parameters to evaluate an optical modulator, one should make a trade-off when determining the operation point of the optical modulator. As shown in Fig. 4(b), when choosing a small Fermi level (i.e. with a low gate voltage), the optical modulator can be ultra-short to achieve an acceptable extinction ratio because of the very high slope of the curve of propagation loss. For example, when choosing V_{G0} = 2.0 V, the propagation loss is ~72.2 dB/μm and an extinction ratio of ~157 dB/μm can be achieved with ΔV_G = −0.5 V. Note that an optical modulator should be long enough (e.g. ~100 nm) for the fabrication in the practical case. Consequently, the insertion loss of the 100-nm-long optical modulator is too high (up to 7.2 dB) to be acceptable. Alternatively, here we choose the operation point as V_{G0} = 7.2 V and ΔV_G = −5.2 V. In this case, one has Real(n_{eff}) = 63.3 and the propagation loss of 4.6 dB/μm when the gate voltage is tuned to $V_G = V_{G0}$ = 7.2 V (on-state, E_{F1} = 0.3 eV). In contrast, one has Real(n_{eff}) = 168.3 and the propagation loss of 72.2 dB/μm when $V_G = V_{G0} + \Delta V_G$ = 2.0 V (off-state, E_{F1} = 0.16 eV). With this design, the optical modulator can be as short as 150 nm to achieve an extinction ratio of ~10 dB and the insertion loss is acceptable (~0.7 dB only). Figure 4(c) displays the simulated light propagation in the designed optical modulator when V_G = 7.2 V, and 2.0 V, respectively. It shows that there is no significant power attenuation when V_G = 7.2 V while light attenuates significantly when V_G = 2.0 V, as expected.

The frequency dependence of the mode properties is also analyzed in the frequency ranging from 30 THz to 45 THz, as shown in Fig. 5. In this calculation, the parameters are chosen as w = 100 nm, d_1 = 60 nm, and d_2 = 40 nm while the Fermi level E_{F1} is assumed to be 0.16 eV, 0.2 eV, 0.3 eV, and 0.4 eV (correspondingly the Fermi level E_{F2} is 0.20 eV, 0.24 eV, 0.37 eV, and 0.49 eV), respectively. As shown in Fig. 5(a) and Fig. 5(b), the fundamental mode has higher propagation loss and larger Real(n_{eff}) at a higher operation frequency for any given Fermi level, which is in agreement with Eq. (2) (see Methods). More importantly, the propagation loss and Real(n_{eff}) of the present GPWG can be modulated in a broad band, so that the present GPWG is available for different operation frequencies. The inset of Figure 5(b) shows that the group velocity of the GPWG

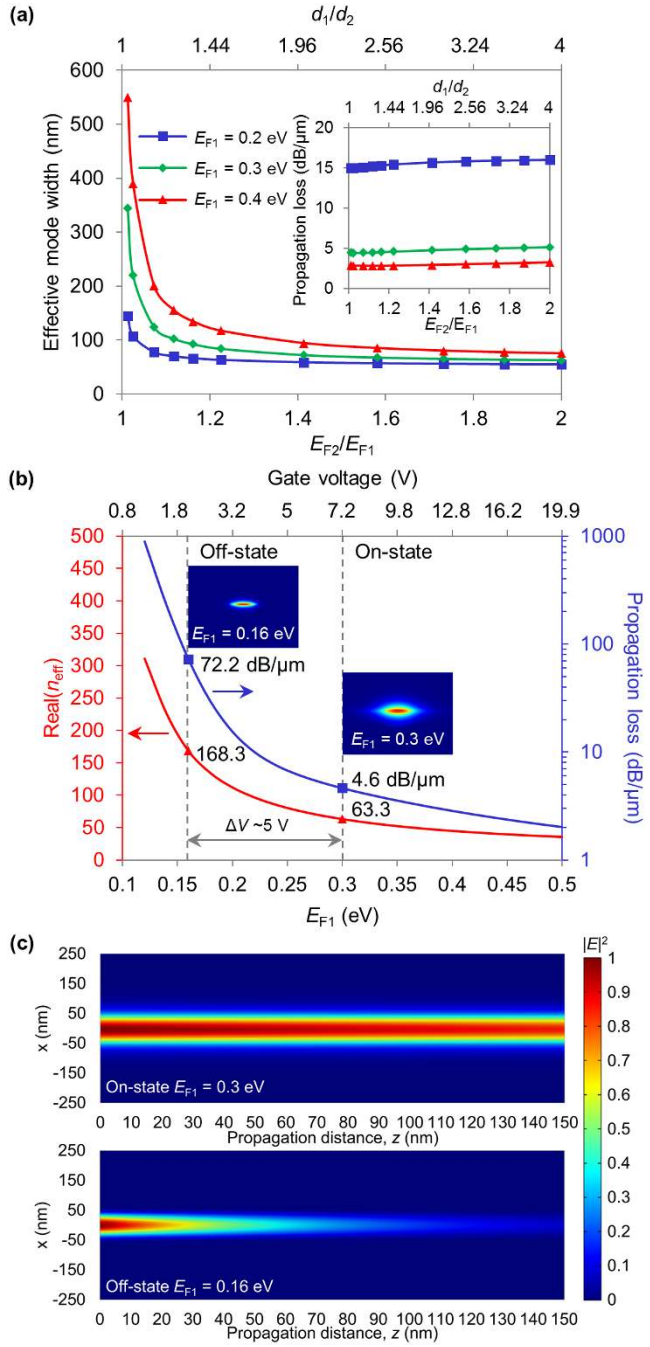

Figure 4 | Fermi level dependence of the mode properties for the proposed GPWG and the application for a GPWG-based optical modulator. (a) The effective mode width and the propagation loss as a function of E_{F2}/E_{F1} for the present GPWG with different Fermi levels in graphene when $w = 100$ nm and $d_2 = 40$ nm. (b) Real(n_{eff}) and the propagation loss of the proposed GPWG as a function of the Fermi level E_{F1} for the core (the gate voltage) when $w = 100$ nm, $d_1 = 60$ nm and $d_2 = 40$ nm. The position of the on-state ($E_{F1} = 0.3$ eV, $V_G = 7.2$ V) and the-off state ($E_{F1} = 0.16$ eV, $V_G = 2$ V) for the proposed optical modulator are marked with grey dashed lines. Insets: Mode profiles for the two states. (c) The normalized light intensity propagation profiles in the designed optical modulator for the on-state and the off-state, respectively.

remains three orders of magnitude slower than the light speed for vacuum in the whole frequency range and can be modified significantly by tuning the Fermi level of graphene. This enables tunable slow light[33], which is useful for many applications[34].

Considering that the evanescent coupling between two parallel optical waveguides is very important for the design of many devices, the evanescent coupling in a system consisting of two identical parallel waveguides is analyzed here. As an example, we choose $d_1 = 60$ nm, $d_2 = 40$ nm, and the Fermi level is assumed as $E_{F1} = 0.22$ eV, 0.25 eV, and 0.3 eV. Figure 6(a) shows the coupling length (defined as the beat length of the two super modes) for the case of $w = 50$ nm as the separation D between the two coupled waveguides varies while Figure 6(b) shows the coupling length for the case of $D = 150$ nm as the core width w varies. As can be seen, the coupling length increases significantly as the separation or the width increases. For example, when $w = 50$ nm, $D = 150$ nm, and $E_{F1} = 0.22$ eV, the coupling length is as long as 50 μm. In this case, the coupling crosstalk is less than −30 dB considering that the device length is usually less than 1 μm. It indicates that an ultra-dense photonic integrated circuit can be achieved. One can also find that the coupling length is very sensitive to the Fermi level of the graphene monolayer, so that it is possible to realize electrically-switched directional coupler.

Here we propose an ultra-compact optical switch based on an asymmetrical directional coupler (ADC) which consists of two optical waveguides with different core widths w_1 and w_2, as shown in Fig. 6(c). In this design, the graphene monolayer on top of the coupling region is split into two parts, between which there is a narrow slot so that the two waveguides can be tuned by applying a gate voltage individually. When the gate voltages applied to the two parts are the same, the Fermi levels for the two parts of graphene are the same and the two waveguides with large width difference will have a big phase mismatch [see Fig. 2(a)]. Consequently, light launched from the input port cannot be cross-coupled from the wide waveguide to the narrow waveguide. On the other hand, when the gate voltage applied to the wider waveguide is optimally higher than that for the narrower one, the phase match condition can be satisfied, so that an efficient cross-coupling from the wide waveguide to the narrow waveguide can be realized by choosing the length of the coupling region appropriately. As an example, we choose $w_1 = 40$ nm, $w_2 = 150$ nm, $d_1 = 90$ nm, $d_2 = 30$ nm, $D = 17.4$ nm, $L_2 = 0.615$ μm, and $L_3 = 0.638$ μm for the ADC optical switch [see Fig. 6(c)]. Here we choose a relatively large ratio d_1/d_2 in order to reduce the unwanted on-state cross-coupling. Fig. 6(d) shows the simulated light propagation in the designed ADC from FEM with the assistance of EIM. It can be seen there is little cross-coupling when the gate voltages for both waveguides are chosen as $V_{G1} = V_{G2} = 10.8$ V (correspondingly the Fermi levels for the two parts of graphene are $E_{F1} = 0.3$ eV). In contrast, an efficient cross-coupling is observed when choosing $V_{G1} = 10.8$ V and $V_{G2} = 14.9$ V (i.e., one has $E_{F1} = 0.3$ eV for the narrow waveguide and $E_{F1} = 0.35$ eV for the wide waveguide). With this design, the extinction ratio of the optical switch is as high as 24 dB while the length of the device is less than 1.25 μm.

Summary

In summary, we have proposed a novel nanoplasmonic waveguide with pattern-free graphene by introducing a spacer with a reversed nano-ridge. The calculations have shown that the easy-to-fabrication GPWG with nanoscale light confinement, relatively low loss, and slowed group velocity enables a significant modulation on the phase shift as well as the propagation loss over a broad band by simply applying a single low bias voltage, which is very helpful for future ultra-dense photonic integrated circuits. The strong light-matter interaction as well as tunable slow light is also of great interest for many applications such as optical nonlinearities. With the proposed GPWG, an ultra-small optical modulator and optical switch have been presented. For the designed optical modulator, the extinction ratio and the insertion loss are 10 dB and 0.7 dB, respectively, while the length is as short as 150 nm (which is attractive for high-speed applications). For the designed optical switch based on an ADC, the

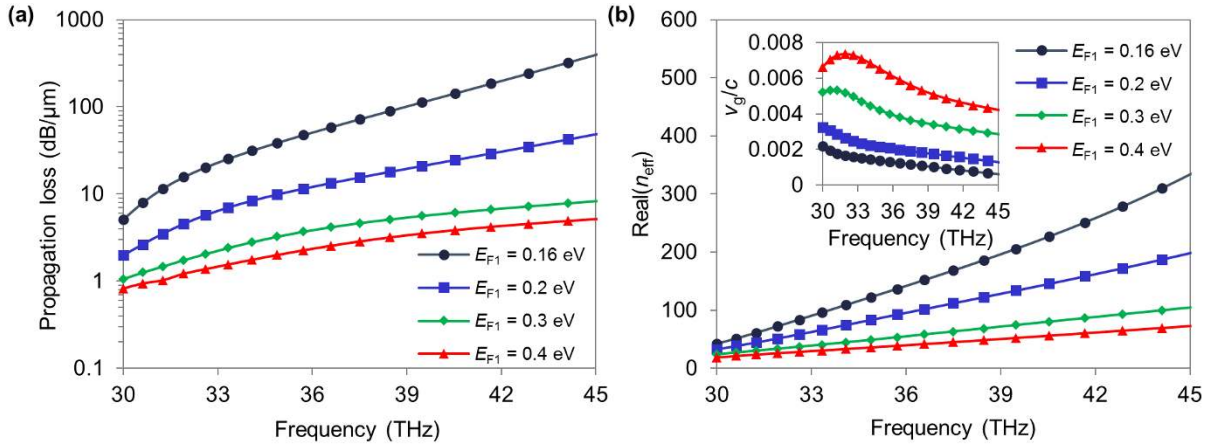

Figure 5 | Frequency dependence of (a) the propagation loss, (b) Real(n_{eff}), and the group velocity (inset) for the proposed GPWG with different Fermi levels in graphene. The structure parameters of the waveguide here is $w = 100$ nm, $d_1 = 60$ nm, $d_2 = 40$ nm. Different bias voltages are applied to achieve different Fermi levels.

device length is 1.25 μm and the extinction ratio is as high as 24 dB. Besides, the GPWG is also useful for other nano devices like spasers owing to the strong localization of photons and electrons deriving from the nonuniform Fermi level distribution of the graphene monolayer.

Methods

Theory. The simulation results presented in this paper are obtained with the frequency-domain finite-element method (FEM) where the graphene monolayer is treated as a thin film with the thickness $t = 1$ nm[9]. The equivalent dielectric constant of graphene is calculated as[9] $\varepsilon = 1 + i\sigma/(\varepsilon_0\omega t)$, where ω is the angular frequency, ε_0 is the vacuum permittivity, and σ is the frequency-dependent optical conductivity of

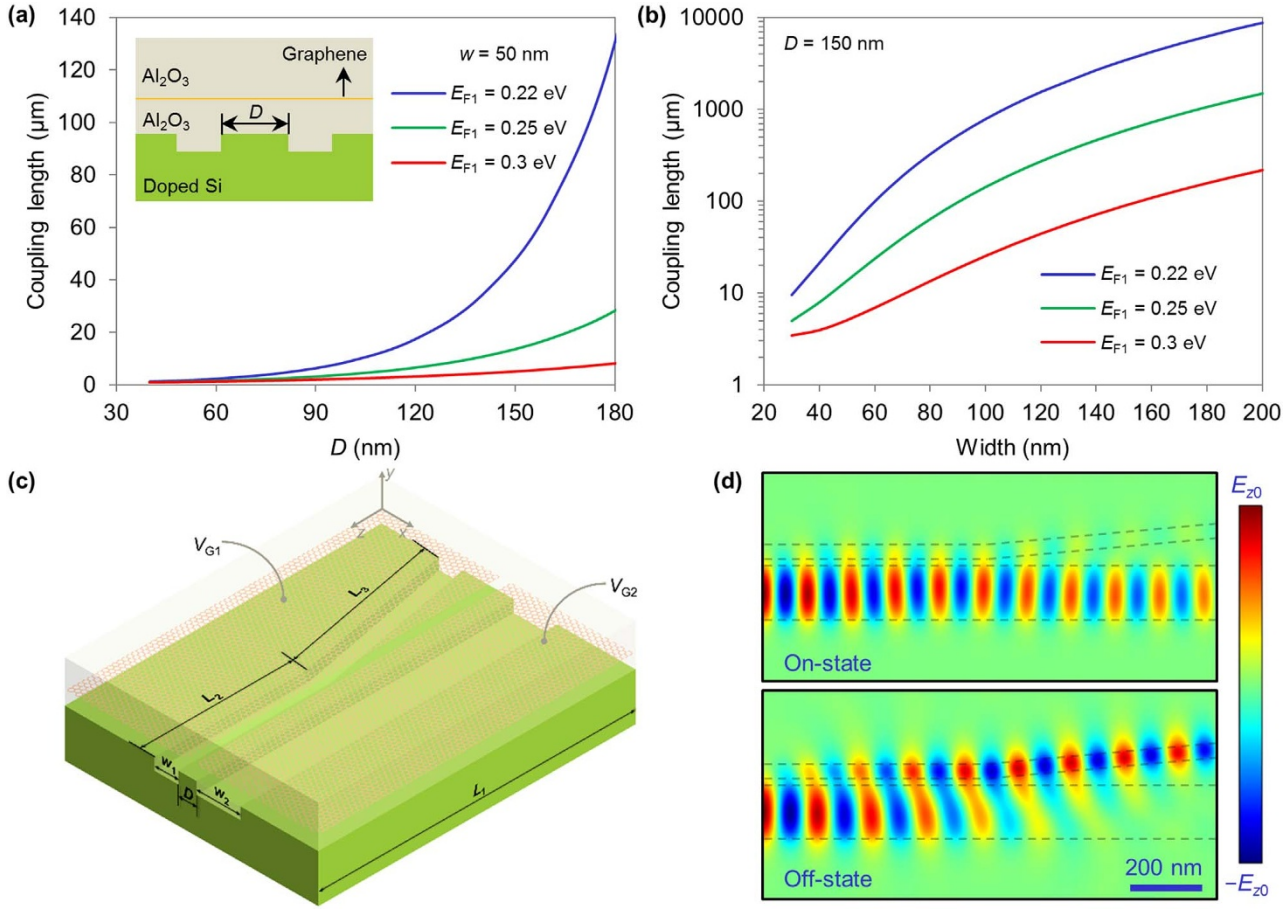

Figure 6 | Coupling between two parallel GPWGs and an ADC optical switch. (a) Coupling length of two identical parallel waveguides as a function of the separation D when $w = 50$ nm, $d_1 = 60$ nm, and $d_2 = 40$ nm. Inset: The schematic of the coupling configuration. (b) Coupling length of two identical parallel waveguides as the waveguide width w varies when $D = 150$ nm, $d_1 = 60$ nm, and $d_2 = 40$ nm. (c) Schematic of the ADC optical switch with $w_1 = 40$ nm, $w_2 = 150$ nm, $d_1 = 90$ nm, $d_2 = 30$ nm, $D = 17.4$ nm, $L_1 = 1.25$ μm, $L_2 = 0.615$ μm, $L_3 = 0.638$ μm. (d) E_z component of the ADC optical switch in the graphene plane for on-state and off-state.

graphene. The optical conductivity σ is given by the expression derived from the Kubo formula[35] and verified by experiments[12] as:

$$\sigma(\omega)=\frac{2ie^2k_BT}{\pi\hbar^2(\omega+i\tau^{-1})}\ln\left[2\cosh(\frac{E_F}{2k_BT})\right]+\frac{ie^2(\omega+i\tau^{-1})}{\pi\hbar^2}\int_0^\infty\frac{f(-\theta)-f(\theta)}{(\omega+i\tau^{-1})^2-4(\theta/\hbar)^2}d\theta, \quad (1)$$

where e is the elementary charge, k_B is the Boltzmann constant, $\hbar$ is the reduced Planck constant, T is the temperature (T= 300 K in this paper), τ is the relaxation time characterizing the plasmon decay attributed to impurities, defects, electron-phonon scattering, and electron-electron interaction[8,10,29], and the Fermi-Dirac distribution $f(\theta)=\{\exp[(\theta-E_F)/k_BT]+1\}^{-1}$. The first term of Eq. (1) is the contribution from intraband transitions and the second term from interband transitions. The Fermi level is given by $E_F=-\mathrm{sgn}(n)\hbar v_F(\pi|n|)^{1/2}$, where the Fermi velocity $v_F\approx 10^6$ m/s, and n is the carrier density. On the basis of a parallel-plate capacitor model, the gate-induced carrier density of graphene is given by $n=-\varepsilon_0\varepsilon_dV_G/ed$, where ε_d and d are the dielectric constant (ε_d= 10 for Al_2O_3) and the thickness of the dielectric spacer, respectively. According to the expression of Fermi level, one has the following relationship $E_F\propto(V_G/d)^{1/2}$. It reveals that the optical conductivity of graphene can be adjusted by varying the carrier-density-dependent Fermi level via e.g. modifying the gate voltage.

As it has been proved theoretically[6–8,10] and experimentally[14,15,17] that SPPs is supportable in a graphene monolayer ranging from THz to MIR spectrum, in this paper we consider the frequency f = 37.5 THz (8 μm in air) with the plasmon energy below that of optical phonons[36] $\hbar\omega_{Oph}\approx$ 0.2 eV (1580 cm^{-1}) and Pauli-blocking interband threshold for properly doped graphene, so both the plasmon damping channel through the emission of an optical phonon with an electron-hole pair and the interband transition are suppressed[6,8,10,29]. In this case, the plasmon lifetime can be reasonably estimated by impurity related DC relaxation time[6,8,10,29] as $\tau=\mu E_F/ev_F^2$(0.5 ps in this paper). Further considering the nonretarded regime ($\beta\gg k_0$ where β is the wavenumber of GPs and k_0 is the vacuum wavenumber) and $E_F\gg k_BT$, the dispersion relationship of GPs for the TM mode in a graphene monolayer is thus approximately[8]

$$\beta(\omega)=\frac{\pi\hbar^2\varepsilon_0(\varepsilon_1+\varepsilon_2)}{e^2E_F}\left(1+\frac{i}{\omega\tau}\right)\omega^2, \quad (2)$$

where ε_1 and ε_2 are the dielectric constants of the dielectric mediums above and underneath graphene. Eq. (2) reveals that the complex SPP effective index $n_{eff}=\beta/k_0$ is inversely proportional to the Fermi level. Since $E_F\propto(V_G/d)^{1/2}$, one will obtain $n_{eff}=\beta/k_0\propto(d/V_G)^{1/2}$. It indicates that GP modes can also be modulated flexibly by tuning the Fermi level.

Effective index method. EIM is the method that deals with a 2D waveguide as an equivalent slab waveguide. As shown in Fig. 3(b), the multilayer structure of the core and the cladding of the 2D waveguide can be equivalent to one kind of material with the TM SPP effective index for the corresponding part and the effective materials compose the core and the cladding of the equivalent slab waveguide. As a result, the characteristics of the 2D waveguide can be simply described by analyzing the TE mode of the equivalent slab waveguide.

1. Barnes, W. L., Dereux, A. & Ebbesen, T. W. Surface plasmon subwavelength optics. *Nature* **424**, 824–830 (2003).
2. MacDonald, K. F. & Zheludev, N. I. Active plasmonics: current status. *Laser Photonics Rev* **4**, 562–567 (2010).
3. Zhao, C. L., Liu, Y. M., Zhao, Y. H., Fang, N. & Huang, T. J. A reconfigurable plasmofluidic lens. *Nat Commun* **4**, 2305 (2013).
4. Kim, J. Joining plasmonics with microfluidics: from convenience to inevitability. *Lab Chip* **12**, 3611–3623 (2012).
5. MacDonald, K. F., Samson, Z. L., Stockman, M. I. & Zheludev, N. I. Ultrafast active plasmonics. *Nat Photonics* 3, 55–58 (2009).
6. Grigorenko, A. N., Polini, M. & Novoselov, K. S. Graphene plasmonics. *Nat Photonics* **6**, 749–758 (2012).
7. Mikhailov, S. A. & Ziegler, K. New electromagnetic mode in graphene. *Phys Rev Lett* **99**, 016803 (2007).
8. Jablan, M., Buljan, H. & Soljacic, M. Plasmonics in graphene at infrared frequencies. *Phys Rev B* **80**, 245435 (2009).
9. Vakil, A. & Engheta, N. Transformation Optics Using Graphene. *Science* **332**, 1291–1294 (2011).
10. Low, T. & Avouris, P. Graphene Plasmonics for Terahertz to Mid-Infrared Applications. *Acs Nano* **8**, 1086–1101 (2014).
11. Wang, F. *et al.* Gate-variable optical transitions in graphene. *Science* **320**, 206–209 (2008).
12. Li, Z. Q. *et al.* Dirac charge dynamics in graphene by infrared spectroscopy. *Nat Phys* **4**, 532–535 (2008).
13. Liu, M. *et al.* A graphene-based broadband optical modulator. *Nature* **474**, 64–67 (2011).
14. Fei, Z. *et al.* Gate-tuning of graphene plasmons revealed by infrared nano-imaging. *Nature* **487**, 82–85 (2012).
15. Chen, J. N. *et al.* Optical nano-imaging of gate-tunable graphene plasmons. *Nature* **487**, 77–81 (2012).
16. Brar, V. W., Jang, M. S., Sherrott, M., Lopez, J. J. & Atwater, H. A. Highly Confined Tunable Mid-Infrared Plasmonics in Graphene Nanoresonators. *Nano Lett* **13**, 2541–2547 (2013).
17. Alonso-Gonzalez, P. *et al.* Controlling graphene plasmons with resonant metal antennas and spatial conductivity patterns. *Science* **344**, 1369–1373 (2014).
18. Christensen, J., Manjavacas, A., Thongrattanasiri, S., Koppens, F. H. L. & de Abajo, F. J. G. Graphene Plasmon Waveguiding and Hybridization in Individual and Paired Nanoribbons. *Acs Nano* **6**, 431–440 (2012).
19. Bolotin, K. I. *et al.* Ultrahigh electron mobility in suspended graphene. *Solid State Commun* **146**, 351–355 (2008).
20. Soref, R. Mid-infrared photonics in silicon and germanium. *Nat Photonics* **4**, 495–497 (2010).
21. Nikitin, A. Y., Guinea, F., Garcia-Vidal, F. J. & Martin-Moreno, L. Edge and waveguide terahertz surface plasmon modes in graphene microribbons. *Phys Rev B* **84**, 161407 (2011).
22. Zhu, X. L., Yan, W., Mortensen, N. A. & Xiao, S. S. Bends and splitters in graphene nanoribbon waveguides. *Optics Express* **21**, 3486–3491 (2013).
23. Forati, E. & Hanson, G. W. Surface plasmon polaritons on soft-boundary graphene nanoribbons and their application in switching/demultiplexing. *Applied Physics Letters* **103**, 133104 (2013).
24. Forati, E. & Hanson, G. W. Soft-boundary graphene nanoribbon formed by a graphene sheet above a perturbed ground plane: conductivity profile and SPP modal current distribution. *J Optics-Uk* **15**, 114006 (2013).
25. He, S. L., Zhang, X. Z. & He, Y. R. Graphene nano-ribbon waveguides of record-small mode area and ultra-high effective refractive indices for future VLSI. *Optics Express* **21**, 30664–30673 (2013).
26. Ooi, K. J. A., Chu, H. S., Ang, L. K. & Bai, P. Mid-infrared active graphene nanoribbon plasmonic waveguide devices. *J Opt Soc Am B* **30**, 3111–3116 (2013).
27. Lao, J., Tao, J., Wang, Q. J. & Huang, X. G. Tunable graphene-based plasmonic waveguides: nano modulators and nano attenuators. *Laser Photonics Rev* **8**, 569–574 (2014).
28. Sun, Y., Zheng, Z., Cheng, J. T. & Liu, J. W. Graphene surface plasmon waveguides incorporating high-index dielectric ridges for single mode transmission. *Opt Commun* **328**, 124–128 (2014).
29. Yan, H. G. *et al.* Damping pathways of mid-infrared plasmons in graphene nanostructures. *Nat Photonics* **7**, 394–399 (2013).
30. Sakai, J. Optical power confinement factor in a Bragg fiber: 1. Formulation and general properties. *J Opt Soc Am B* **24**, 9–19 (2007).
31. Xia, J. L., Chen, F., Li, J. H. & Tao, N. J. Measurement of the quantum capacitance of graphene. *Nat Nanotech* **4**, 505–509 (2009).
32. Lovat, G., Hanson, G. W., Araneo, R. & Burghignoli, P. Semiclassical spatially dispersive intraband conductivity tensor and quantum capacitance of graphene. *Phys Rev B* **87**, 115429 (2013).
33. Chen, P. Y., Argyropoulos, C. & Alu, A. Terahertz Antenna Phase Shifters Using Integrally-Gated Graphene Transmission-Lines. *Ieee T Antenn Propag* **61**, 1528–1537 (2013).
34. Krauss, T. F. Why do we need slow light? *Nat Photonics* **2**, 448–450 (2008).
35. Gusynin, V. P., Sharapov, S. G. & Carbotte, J. P. Unusual microwave response of Dirac quasiparticles in graphene. *Phys Rev Lett* **96**, 256802 (2006).
36. Ferrari, A. C. *et al.* Raman spectrum of graphene and graphene layers. *Phys Rev Lett* **97**, 187401 (2006).

Acknowledgments

This project was partially supported by the Nature Science Foundation of China (No. 11374263, and 61422510), the Doctoral Fund of Ministry of Education of China (No. 20120101110094).

Author contributions

J.Z. proposed the waveguide structure. J.Z., L.Y. and D.D. discussed the modal analysis and calculation. J.Z., D.D. and S.H. contributed to the scientific discussions and the manuscript writing/revision. D.D. supervised the whole project funded and finalized the paper.

Additional information

Competing financial interests: The authors declare no competing financial interests.

How to cite this article: Zheng, J., Yu, L., He, S. & Dai, D. Tunable pattern-free graphene nanoplasmonic waveguides on trenched silicon substrate. *Sci. Rep.* 5, 7987; DOI:10.1038/srep07987 (2015).